Semiconductor Physics, Quantum Electronics & Optoelectronics, 2015. V. 18, N 4. P. 385-390.
doi: 10.15407/spqeo18.04.385

PACS 42.70.Gi, 68.65.Ac, 81.15.Fg

Photo-induced effects in $(Ag_3AsS_3)_{0.6}(As_2S_3)_{0.4}$ thin films and multilayers with gold nanoparticles

Yu.Yu. Neimet[1], I.P. Studenyak[1], M.Yu. Buchuk[1], R. Bohdan[2], S. Kökényesi[2], L. Daróci[2], P. Nemec[3]
[1]*Uzhhorod National University, Faculty of Physics,*
3, Narodna Sq., 88000 Uzhhorod, Ukraine
[2]*University of DEBIrecen, Faculty of Science and Technology,*
18/a Bem Sq., 4026 DEBIrecen, Hungary
[3]*University of Pardubice, Department of General and Inorganic Chemistry,*
95 Studentská, 53210 Pardubice, Czech Republic
E-mail: studenyak@dr.com

Abstract. $(Ag_3AsS_3)_{0.6}(As_2S_3)_{0.4}$ single layer thin films, as well as ones deposited onto glass substrates previously covered with gold nanoparticle (GNP) layers were studied. Conventional thermal evaporation and pulse laser deposition techniques were used to deposit chalcogenide films onto previously prepared GNP layer. Roughness analysis of as-deposited film surfaces was performed. The influence of laser (LI) and e-beam (EBI) irradiation on structural and optical properties was analysed. Single layer films as well as sandwich structures with GNP on their base were found to be sensitive to LI and EBI. Irradiations caused growth of additional structures at films surfaces which was enhanced by a presence of gold.

Keywords: thin film, rapid thermal evaporation, pulse laser deposition, photo-induced effect, SEM, AFM, e-beam, gold nanoparticles.

Manuscript received 20.05.15; revised version received 19.08.15; accepted for publication 28.10.15; published online 03.12.15.

1. Introduction

Semiconducting glasses and films based on amorphous chalcogenides with addition of metallic atoms or compounds (including the crystalline ones) have been extensively studied owing to various current and future possible applications [1-4]. From this viewpoint, Ag-As-S films are considered as suitable materials for optical recording, electrochemical sensing, as photoresistive materials, *etc.* [5, 6]. Numerous experiments have been performed with chalcogenide bulk glasses, thin films and nanomultilayers in order to investigate structural, compositional and surface changes as a result of laser and e-beam irradiation [7-9].

In the recent years, surface plasmon resonance (SPR) of gold nanoparticles (GNP) has been widely used to enhance photo-structural changes in chalcogenide binary systems, namely in As-Se (most often $As_{20}Se_{80}$ because of its maximal photo sensitivity in As-Se system [7]) and As-S (As_2S_3) thin films, which is caused by laser light [10-12]. Action of light simultaneously absorbed by chalcogenide layers and surface plasmons of GNP can enhance structural transformations in chalcogenide layers [10], as well as influences on their surfaces [12]. For optimization, one needs to create a structure with SPR occurring in the spectral range of maximum sensitivity in materials under investigation (e.g., in the range of the optical absorption edge), which can be achieved by variation of the GNP sizes, different compositions of thin film materials and methods used for creation of the structures.

Therefore, it is now of a certain interest to study such effects in the Ag-As-S thin films obtained by two

Semiconductor Physics, Quantum Electronics & Optoelectronics, 2015. V. 18, N 4. P. 385-390.
doi: 10.15407/spqeo18.04.385

distinct technologies, i.e. rapid thermal evaporation (RTE) and pulse laser deposition (PLD). In the recent time, $(Ag_3AsS_3)_{0.6}(As_2S_3)_{0.4}$ composite thin films prepared by RTE [13-15] and PLD [16] have been already investigated by our group. Surface patterning on As(Ge)-S(Se) amorphous chalcogenide nanomultilayers obtained using the latter two methods was investigated recently [8]. Mass transport was demonstrated due to laser (LI) and e-beam (EBI) irradiation influence, and this effect was used for creation patterns of valleys (LI) and squares (EBI) [8]. Thus, the present paper is devoted to investigation of photo-induced behavior of $(Ag_3AsS_3)_{0.6}(As_2S_3)_{0.4}$ thin films, as well as to study of gold plasmon field influence on their structure and optical properties.

2. Experimental

Synthesis of the initial $(Ag_3AsS_3)_{0.6}(As_2S_3)_{0.4}$ bulk composite was carried out from previously synthesized Ag_3AsS_3 and As_2S_3 compounds at the temperature 700 °C for 24 h with following melt homogenization for 72 h. $(Ag_3AsS_3)_{0.6}(As_2S_3)_{0.4}$ composite was observed to contain $AgAsS_2$ and Ag_3AsS_3 microcrystalline inclusions in a glassy As_2S_3 host matrix [17].

Gold nanoparticles were obtained on the silica glass substrates by annealing of thin gold films previously deposited using thermal evaporation [10]. Subsequently, the GNP layers were covered with the $(Ag_3AsS_3)_{0.6}(As_2S_3)_{0.4}$ thin films deposited by rapid thermal evaporation (RTE) and pulse laser deposition (PLD) techniques.

Structural properties of thin films under investigation were studied using the Hitachi S-4300 scanning electron microscope (SEM). Energy-dispersive X-ray spectroscopy (EDX) within SEM was used to ensure chemical composition of thin films**.** The thickness of these films was measured using the Ambios Stylus XP-1 profile meter. Thicknesses of as-prepared $(Ag_3AsS_3)_{0.6}(As_2S_3)_{0.4}$ thin films were estimated to be 600 and 530 nm for the RTE and PLD techniques, respectively; initial GNP layers were obtained being of the 50-nm thickness. The Veeco diCaliber Nanoscope 3100 atomic force microscope (AFM) was used to obtain profiles of the surfaces and to calculate root mean square (RMS) surface roughness R_q of the films.

Optical transmission spectra $T(\lambda)$ of thin films were studied at room temperature using Shimatzu UV-3600 spectrophotometer. Green (λ = 532 nm, output power P = 20 mW) and red (λ = 650 nm, output power P = 6.7 mW) diode pumped semiconductor lasers were used for LI of prepared samples. Intensities of laser beams were checked using ThorLabs PM100 power meter setup. EB within SEM with accelerated voltage U = 5 kV and electron emission currents I_e = 10 μA (for RTE) and I_e = 6…7 μA (for PLD) were used to irradiate the samples.

3. Results and discussion

3.1. Structure and surfaces

Fig. 1 presents SEM images of as-prepared $(Ag_3AsS_3)_{0.6}(As_2S_3)_{0.4}$ thin films and sandwich structures of chalcogenide films with GNP layers in the bottom. Figs. 1a, 1b show that thin films deposited by RTE have numerous particles of different shapes at a flat surface of a base film layer. EDX method has shown these films to be enriched with arsenic and have a deficiency of sulphur in comparison with the initial bulk composite used for deposition. Moreover, rather high excess of silver is found in the atomic composition of particles found at the surface. Particles that cover the RTE film with GNP in the bottom (let's abbreviate these structures using shortening RTE+GNP) (Fig. 1b) have about twice larger amount of silver and twice lower of sulfur in its chemical composition than those of a pure RTE film (Fig. 1a). Contrary to RTE, the PLD films are obtained non-homogeneous with numerous raindrop-like bubbles at the surface (Figs. 1c, 1d). In comparison with the RTE film, the PLD films have smaller and rougher flat regions (Fig. 1c). In the same way as for cones at the RTE films, the bubbles observed at the surface of the PLD films have increased silver content. Particles (RTE) and bubbles (PLD) have nearly the same sulphur content. Opposite to particles in the case of the RTE films, bubbles have an increased As-content comparing to that of the base PLD thin film.

Obviously, sandwich structures containing GNP layers have pronounced bigger roughness of the flat areas, whereas the prominent structures and bubbles are smoothed down (Figs. 1b, 1d). Fig. 2 shows the three-dimensional AFM images of the $(Ag_3AsS_3)_{0.6}(As_2S_3)_{0.4}$ films and sandwiches surfaces, which evidences in favour of the latter fact. The roughness analysis was performed and root mean square roughness (RMS) R_q was estimated from AFM images with 3-μm scan range

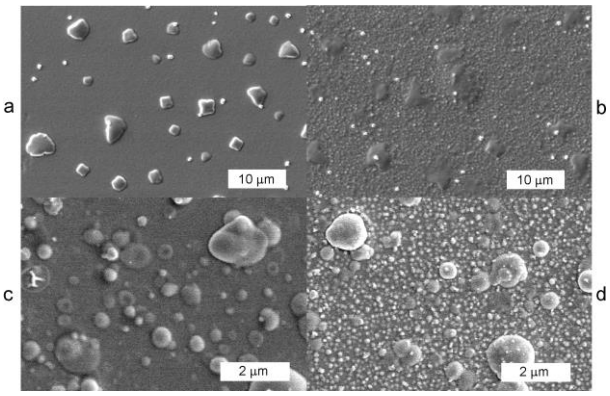

Fig. 1. SEM images of as-deposited single layer $(Ag_3AsS_3)_{0.6}(As_2S_3)_{0.4}$ thin films (a, c) and sandwich structures with GNP (b, d) prepared using the RTE (a, b) and PLD (c, d) techniques.

Semiconductor Physics, Quantum Electronics & Optoelectronics, 2015. V. 18, N 4. P. 385-390.
doi: 10.15407/spqeo18.04.385

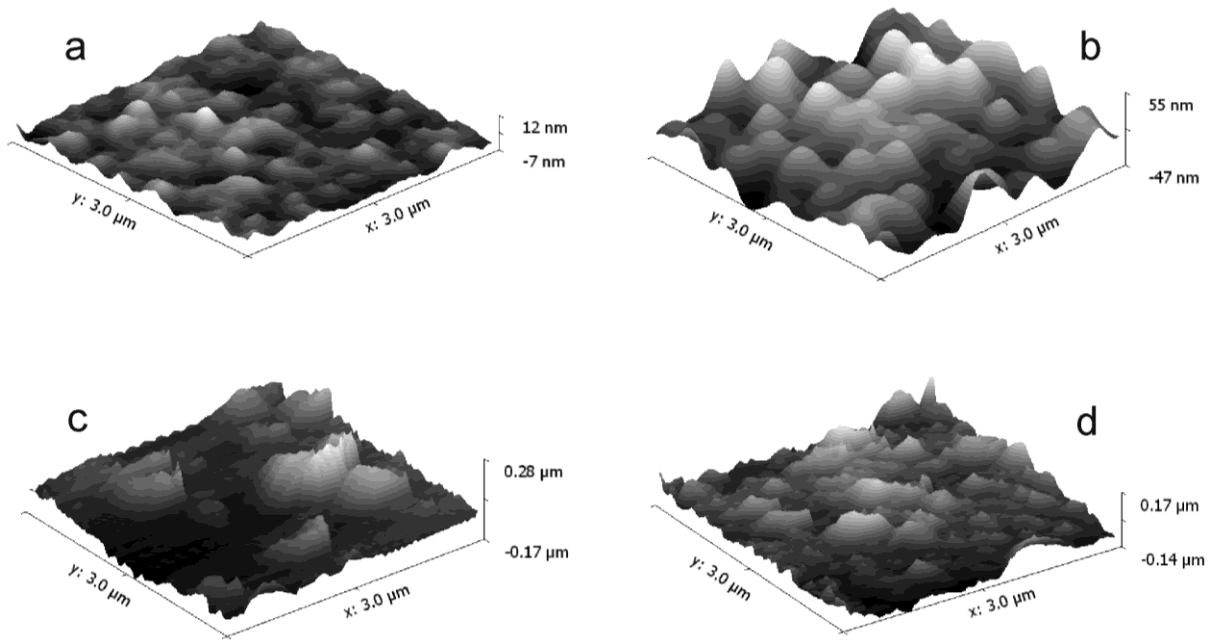

Fig. 2. Three-dimensional AFM images of as-deposited single layer $(Ag_3AsS_3)_{0.6}(As_2S_3)_{0.4}$ thin films (a, c) and sandwich structures with GNP (b, d) prepared using the RTE (a, b) and PLD (c, d) techniques.

(Fig. 2). It is shown that the average R_q value is lower for the films prepared using RTE (R_q = 2.5 nm), comparing to the films prepared using PLD (R_q = 64.7 nm). Further to be mentioned, the RTE films with the GNP ones have higher R_q = 18.0 nm comparing to that of the films without Au. Different situation can be seen for the PLD film, where addition of the GNP layer decreases the RMS roughness (R_q = 42.7 nm).

3.2. Laser irradiation

Fig. 3 shows the optical transmittance of as-deposited $(Ag_3AsS_3)_{0.6}(As_2S_3)_{0.4}$ thin films produced by the RTE and PLD techniques, together with transmittance data concerning sandwiches with GNP. Spectra of single gold nanoparticle layers, used in sandwich structures with RTE and PLD films are also presented in Fig. 3. It was revealed that the most probably minima at the GNP spectra corresponding to the plasmon resonance frequencies of gold for both sandwiches with RTE and PLD films are shifted to longer wavelengths in the sandwich structures with GNP, thus resulting in reducing the transmittance peaks of single chalcogenide layers (Fig. 3).

It is known that the samples with gold nanoparticles satisfy the conditions for surface plasmon resonance excitation in green-red spectral region [11]. In this spectral region, As_2S_3 has maximum sensitivity to photo-induced transformations. In our case, optical absorption edge of the prepared using PLD technique $(Ag_3AsS_3)_{0.6}(As_2S_3)_{0.4}$ thin film, as well as a sandwich with GNP, is shifted to longer wavelength and behaves itself differently under the influence of green (532 nm) and red (633 nm) laser near band-gap light (emission lines of the lasers are shown by vertical dotted lines in Fig. 3).

It is shown that both single films and sandwich structures prepared using the RTE and PLD techniques are sensitive to laser irradiation. Fig. 4 presents time dependences of relative transmitted light intensity during the laser irradiation of green laser in RTE (curve *1*) and PLD (curve *3*) single layers and in sandwiches with GNP (curves *2* and *4*, respectively).

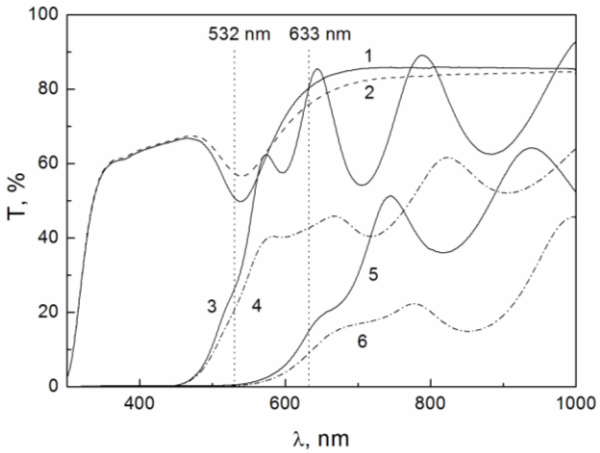

Fig. 3. Optical transmission of as-deposited GNP layers (*1*, *2*), RTE (*3*) and PLD (*5*) $(Ag_3AsS_3)_{0.6}(As_2S_3)_{0.4}$ thin films, and sandwich structures with GNP (*4*, *6*). Vertical lines show emission wavelengths of green (532 nm) and red (633 nm) lasers used for irradiation of the samples.

Semiconductor Physics, Quantum Electronics & Optoelectronics, 2015. V. 18, N 4. P. 385-390.
doi: 10.15407/spqeo18.04.385

Table. Rates of photo-induced changes, $\gamma = \Delta(I/I_0)/\Delta t$ (in s^{-1}), under the influence of green laser light with irradiation times, Δt. Sign (–) denotes photo-darkening effect. Otherwise photo-bleaching effect is meant to be observed.

Δt, s	γ, s^{-1}			
	RTE	RTE+GNP	PLD	PLD+GNP
50	(–) $1.6\cdot10^{-3}$	$8.0\cdot10^{-4}$	$6.0\cdot10^{-3}$	$3.8\cdot10^{-3}$
150	(–) $3.0\cdot10^{-4}$	$2.6\cdot10^{-3}$	$4.1\cdot10^{-3}$	$2.4\cdot10^{-3}$

Photo-darkening with subsequent photo-bleaching effect due to LI was detected for the RTE single layers (Fig. 4, curves *1* and *2*). At the same time, the gold layer removes photo-darkening, so that the only photo-bleaching effect remains at the very beginning of irradiation. It can be also seen that presence of GNP slightly enhances photo-induced changes of relative transmittance I/I_0. Relation of transmitted laser beam intensity, I, to an intensity of incident laser beam, I_0, depending on time of laser illumination, t, yields $\gamma = \Delta(I/I_0)/\Delta t$, which has been taken as a rate of photo-induced changes. These rates were estimated for all the investigated films and presented in Table.

At the wavelength of green laser emission (λ = 532 nm), the investigated PLD films were shown to absorb light (see Fig. 3). Nevertheless, time dependences of the relative transmitted light intensity during illumination of green laser show an increase of relation I/I_0 by more than 70% (Fig. 4, curve *3*). LI with red laser in this case shows no significant effect upon the film. In the case of the PLD+GNP sandwich structure, opposite to the RTE+GNP, presence of the GNP layer in the bottom of the chalcogenide PLD film causes lowering the I/I_0 change (Fig. *4*, curve *4*).

It should be noted that the maximal photo-induced change (particularly, darkening) with the rate of $\gamma = (-)1.4\cdot10^{-2}$ s^{-1} is observed for the RTE film irradiated using the green laser and can be observed in the first 7 seconds of LI (Fig. 4, curve *1*). After this time, the film starts bleaching. Earlier, similar effect was observed for sandwich structures based on $As_{20}Se_{80}$ thin films with GNP [10, 11]. In the case of LI with red laser, the PLD films exhibit an increase at about 2% for both pure PLD layer and for the structure with GNP.

Inset to Fig. 4 represents time dependence of the relative transmitted light intensity during green (532 nm) LI of the sandwich structure PLD+GNP and subsequent switching on the additional red (650 nm) laser in the scheme of lateral supplementary illumination. A sudden drop of transmittance was observed as a result of additional red LI with subsequent transmittance, which returns after switching off the supplementary laser. This effect is interesting from the applicability point of view, and thus, for instance, can be used as a trigger in all-optical switch devices.

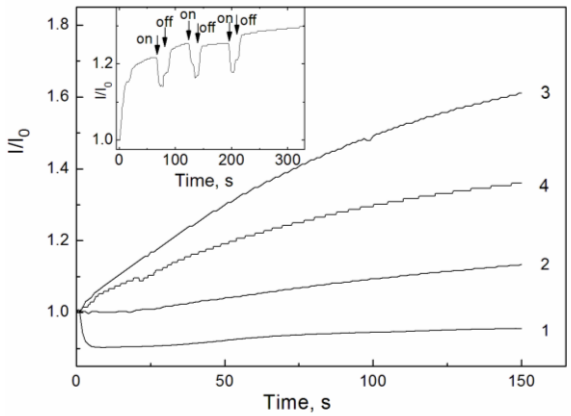

Fig. 4. Time dependences of relative transmitted light intensity during illumination of green (533 nm, output power P = 100 mW) laser in single layer RTE (*1*) and PLD (*3*) thin films and in sandwich structures with GNP (*2*, *4*, respectively). Inset shows time dependence of relative transmitted light intensity during green (533 nm) and subsequent red (650 nm) laser illuminations of the sandwich structure PLD+GNP.

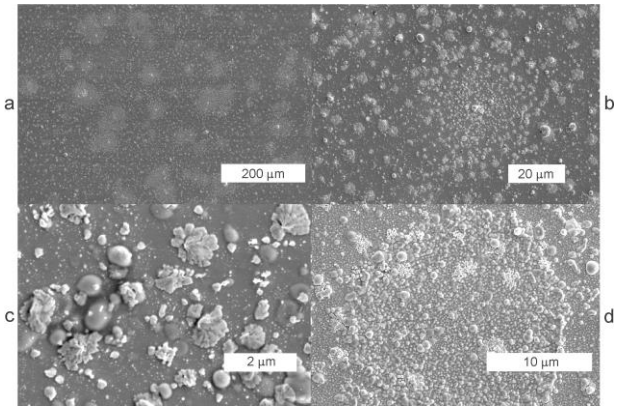

Fig. 5. SEM images of as-prepared PLD single layer $(Ag_3AsS_3)_{0.6}(As_2S_3)_{0.4}$ thin films (a, b, c) and a film in a sandwich with GNP (d) irradiated with the green laser at λ = 533 nm through the 1.2-mm diaphragm.

Fig. 5 shows the SEM images of single layer prepared by the PLD technique (a, b, c) and in a sandwich with GNP (d) $(Ag_3AsS_3)_{0.6}(As_2S_3)_{0.4}$ thin films, irradiated with the green laser at λ = 533 nm through 1.2 mm diaphragm. Comparing to as-deposited PLD films, presented in Fig. 1, one can observe presence of numerous circular-shaped areas of grown-up structures, which coagulate in islets (Figs. 5a, 5b). It should be noted that the addition of gold enhances growth of these structures due to LI (Fig. 5d).

3.3. E-beam irradiation

Fig. 6 shows SEM image of e-beam irradiated for up to 180 seconds sandwich of the RTE $(Ag_3AsS_3)_{0.6}(As_2S_3)_{0.4}$ thin film with GNP layer. One can observe elevation of

Semiconductor Physics, Quantum Electronics & Optoelectronics, 2015. V. 18, N 4. P. 385-390.
doi: 10.15407/spqeo18.04.385

the surface due to electron beam. In Fig. 7, the results of EDX analysis are presented, which helped to reveal abrupt increase of the arsenic content and slight increase of the selenium content due to EBI for the first 30 seconds of irradiation. Later, at incremented up to 180 s times, As and S contents decrease. As we can see, the silver content behaves independently (no alteration after the first 30 s), continuously increasing during EBI. We can see results of silver content increase at the image in Fig. 6, where silver ions Ag^+ or silver enriched compounds are pulled out of the film volume. It's a most likely that this process takes place due to driving electric force originating from the negative electron beam.

Fig. 8 demonstrates surface evolution during EBI of the sandwich structure containing PLD $(Ag_3AsS_3)_{0.6}(As_2S_3)_{0.4}$ thin film together with a GNP layer. SEM images in Fig. 8 manifest the whisker growth from a teardrop-shaped Ag-enriched particle, as well as appearance of the other smaller particles that are pulled out from the films volume as a result of EBI. One should mention that, in the case of PLD+GNP structures,

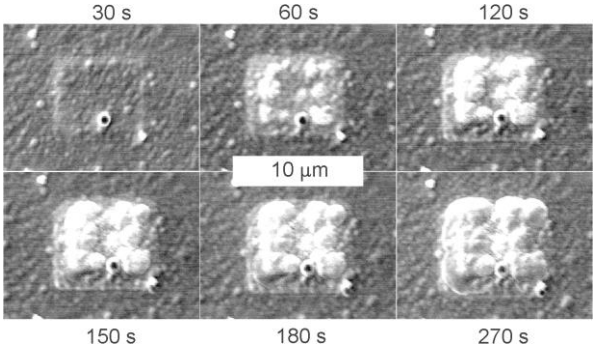

Fig. 6. SEM images of the e-beam irradiated sandwich structure of the RTE $(Ag_3AsS_3)_{0.6}(As_2S_3)_{0.4}$ thin film with GNP layer at increased irradiation times.

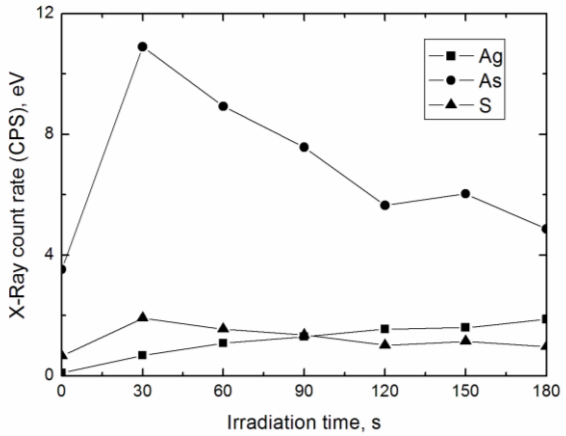

Fig. 7. X-ray count rate of the constituent elements in the RTE $(Ag_3AsS_3)_{0.6}(As_2S_3)_{0.4}$ thin film versus the e-beam irradiation time, obtained using EDX technique within SEM.

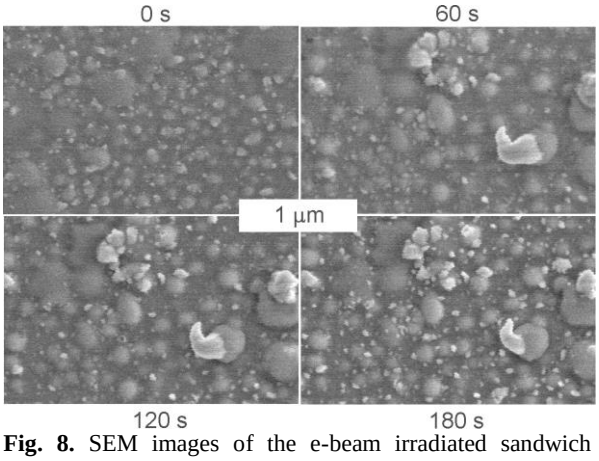

Fig. 8. SEM images of the e-beam irradiated sandwich structure of the PLD $(Ag_3AsS_3)_{0.6}(As_2S_3)_{0.4}$ thin film with GNP layer at increased irradiation times.

the images show scanning along the whole area, contrary to RTE+GNP, where squares of 4×6 μm were irradiated. Moreover, EBI of lower emission current (i.e., I_e = 6…7 μA) was used to irradiate the PLD+GNP sample, as for RTE+GNP structures (I_e = 10 μA). Nevertheless, we revealed the different behaviour of sandwiches with PLD and RTE films due to EBI. Obviously, more homogeneous distribution of Ag in the RTE films gives elevation of the whole irradiated area (Fig. 6), whereas whiskers start to form from Ag-enriched bubbles in the PLD films.

4. Conclusions

$(Ag_3AsS_3)_{0.6}(As_2S_3)_{0.4}$ thin films deposited onto glass substrates previously covered with GNP layers were investigated. RTE and PLD deposition techniques were used for obtaining the above mentioned thin films. Roughness analysis showed that sandwich structures containing GNP layer have a pronounced bigger roughness of flat areas at the surfaces, whereas prominent structures and bubbles of as-deposited films are smoothed down.

Both single films and sandwich structures prepared using the RTE and PLD techniques are sensitive to laser and e-beam illuminations. Treating the obtained structures with LI and EBI causes growth of additional structures at film surfaces, while gold appreciably enhances these effects. Photo-darkening with subsequent photo-bleaching effect due to LI was detected for the single layered RTE samples, while gold layer removes photo-darkening effect, so that the only photo-bleaching remains. Time dependences of the relative transmitted light intensity (I/I_0) during illumination with the green laser show an increase of I/I_0 by more than 70%. Opposite to RTE+GNP, presence of the GNP layer in the bottom of the PLD film causes lowering of I/I_0 change. A sudden drop of transmittance was observed as a result

of additional red LI usage, while irradiating the PLD+GNP structures with the green laser. Subsequent transmittance back-off was observed after switching the supplementary red laser off. Elevation of the surface and increase of the Ag-content were observed due to EBI of RTE thin films and RTE+GNP structures. Whisker growth and appearance of other smaller particles over the surface are results of EBI irradiation of the PLD+GNP structures.

The above mentioned effects can be probably used in all-optical switching devices as well as can improve optical recording. EBI effects upon RTE+GNP structures are interesting from the viewpoint of data storage applicability, creation of diffraction gratings, micro-optical elements, *etc*.

Acknowledgements

Mykhailo Buchuk (contract number 51501900) is very much grateful to the International Visegrad Fund scholarship for funding the study.

References

1. T. Ohta, Phase-change optical memory promotes the DVD optical disc // *J. Opt. Adv. Mat.* **3**, p. 609-626 (2001).
2. M. Frumar, Z. Cernosek, J. Jedelsky, B. Frumarova, T. Wagner, Photoinduced changes of structure and properties of amorphous binary and ternary chalcogenides // *J. Opt. Adv. Mat.* **3(2)**, p. 177-188 (2001).
3. M.N. Kozicki, M. Mitkova, M. Park, M. Balakrishnan, G. Gopalan, Information storage using nanoscale electrodeposition of metal in solid electrolytes // *Superlattices and Microstructures* **34**, p. 459-465 (2003).
4. M.N. Kozicki and M. Mitkova, Mass transport in chalcogenide electrolyte films – materials and applications // *J. Non-Cryst. Solids*, **352**, p. 567-577 (2006).
5. M. Frumar and T. Wagner, Ag-doped chalcogenide glasses and their applications // *Cur. Op. in Solid State and Mat. Sci.* **7**, p. 117-126 (2003).
6. R.E. Belford, E. Hajto and A.E. Owen, The selective removal of the negative high-resolution photoresist system Ag-As-S // *Thin Solid Films*, **173**, p. 129-137 (1989).
7. M.L. Trunov, P.M. Nagy, V. Takats, P.M. Lytvyn, S. Kökényesi, E. Kalman, Surface morphology of as-deposited and illuminated As–Se chalcogenide thin films // *J. Non-Crystal. Solids*, **355**, p. 1993-1997 (2009).
8. V. Takats, P. Nemec, A.C. Miller, H. Jain, S. Kökényesi, Surface patterning on amorphous chalcogenide nanomultilayers // *Opt. Mater.* **32**, p. 677-679 (2010).
9. C. Cserhati, S. Charnovych, P.M. Lytvyn, M.L. Trunov, D.L. Beke, Yu. Kaganovskii, S. Kökényesi, E-beam induced mass transport in amorphous $As_{20}Se_{80}$ films // *Mater. Lett.* **85**, p. 113-116 (2012).
10. S. Charnovych, S. Kökényesi, Gy. Glodan and A. Csik, Enhancement of photoinduced transformations in amorphous chalcogenide film via surface plasmon resonances // *Thin Solid Films*, **519**, p. 4309-4312 (2011).
11. S. Charnovych, N. Dmitruk, N. Yurkovich, M. Shiplyak, S. Kökényesi, Photo-induced changes in a-As_2S_3/gold nanoparticle composite layer structures // *Thin Solid Films*, **548**, p. 419-424 (2013).
12. S. Charnovych, I.A. Szabó, A.L. Tóth, J. Volk, M.L. Trunov, S. Kökényesi, Plasmon assisted photoinduced surface changes in amorphous chalcogenide layer // *J. Non-Crystal. Solids*, **377**, p. 200-204 (2013).
13. I.P. Studenyak, Yu.Yu. Neimet, Y.Y. Rati, O.Ye. Petrachenkov, A.M. Solomon, S. Kökényesi, L. Daróci, R. Bogdán, Deposition and structure $(Ag_3AsS_3)_{0.6}(As_2S_3)_{0.4}$ thin films // *Physics and Chemistry of Solid State*, **15 (3)**, p. 504-509 (2014).
14. I.P. Studenyak, Yu.Yu. Neimet, Y.Y. Rati, D. Stanko, M. Kranjčec, S. Kökényesi, L. Daróci, R. Bohdan, Structural and optical studies of $(Ag_3AsS_3)_{0.6}(As_2S_3)_{0.4}$ thin films deposited at different technological conditions // *Semiconductor Physics, Quantum Electronics & Optoelectronics* **17**(3), p. 232-236 (2014).
15. I.P. Studenyak, Yu.Yu. Neimet, Y.Y. Rati, D. Stanko, M. Kranjčec, S. Kökényesi, L. Daróci, R. Bohdan, Structural and optical properties of annealed and illuminated $(Ag_3AsS_3)_{0.6}(As_2S_3)_{0.4}$ thin films // *Opt. Mat.* **37**, p. 718-723 (2014).
16. I.P. Studenyak, M.M. Kutsuk, Y.Y. Rati, V.Yu. Izai, S. Kökényesi, L. Daróci, R. Bohdan, Temperature studies of optical parameters in $(Ag_3AsS_3)_{0.6}(As_2S_3)_{0.4}$ thin films // *Semiconductor Physics, Quantum Electronics & Optoelectronics*, **18**(2), p. 188-192 (2015).
17. I.P. Studenyak, Yu.Yu. Neimet, M. Kranjčec, A.M. Solomon, A.F. Orliukas, A. Kežionis, E. Kazakevičius, T. Šalkus, Electrical conductivity studies in $(Ag_3AsS_3)_x(As_2S_3)_{1-x}$ superionic glasses and composites // *J. Appl. Phys.* **115**, p. 033702-1−033702-5 (2014).